Climate Dynamics
https://doi.org/10.1007/s00382-022-06345-7

Bayesian retro- and prospective assessment of CMIP6 climatology in Pan Third Pole region

Zhu Liu[1,2,3] · Qingyun Duan[1,2,3] · Xuewei Fan[4] · Wentao Li[1,2,3] · Jina Yin[1,5]

Received: 27 November 2021 / Accepted: 6 May 2022

Abstract
Pan Third Pole (PTP) region includes Tibet Plateau (TP), Central Asia (CA) and Southeast Asia (SEA) and it is one of the places on earth that are most sensitive to climate change. Meanwhile, PTP origins a series of large rivers such as Yangtze River, Yellow River and Lancang-Mekong River, which feed millions of people downstream. Therefore, climate change in PTP has significant impact on livings and water supply of local residents. In this study, 16 model predictions from the Coupled Model Inter-comparison Project Phase 6 (CMIP6) and Climate Research Unit (CRU) observations are used to evaluate historical precipitation and temperature climatology changes in PTP region for the far (1901–1930), middle (1941–1970) and near history (1981–2010) respectively. In addition, Bayesian model averaging (BMA) approach is applied to obtain the multi-model weighted average prediction and the BMA values are further used to assess the climate variabilities in the near (2021–2050), middle (2046–2075) and far future (2071–2100) under four SSP-RCP scenarios. Results indicate that temperature is significantly underestimated by most CMIP6 models in TP especially IPSL-CM6A-LR and CanESM5 whereas precipitation is overestimated for CA and TP. Most CMIP6 models do not predict precipitation very well in SEA, the difference of annual total precipitation between the highest estimation from UKESM1-0-LL and the lowest estimation from CAMS-CSM1-0 is about 800 mm. Overall, BMA prediction is more reliable compared with individual models. In addition, Pan Third Pole region is projected to be warmer and wetter in the future and the trend is stronger under SSP5-8.5 scenario. The BMA predicted temperature uncertainty is larger for high latitude CA region whereas precipitation uncertainty is higher for low latitude SEA region.

Keywords CMIP6 · Model bias · Bayesian model averaging · Pan Third Pole · Climatology

1 Introduction

The earth has witnessed significant climate change in the last a few decades (Change 2007; Fan et al. 2021b; Knutti et al. 2016; Liu et al. 2021; Sun et al. 2020). According to the recently released Intergovernmental Panel on Climate Change (IPCC) Assessment Report 6, global surface temperature in the first two decades of the 21st century (2001–2020) was 0.99 °C (ranges 0.84–1.10 °C) higher than 1850–1900. In addition, continued unconstrained intensification in greenhouse gas emissions are likely to result in global warming that substantially exceeds the internationally agreed-upon target of 2 °C above the pre-industrial level (Diffenbaugh and Giorgi 2012). Climate change-induced extreme weather and disasters such as floods, droughts and heatwaves have caused severe productivity and life losses, particularly in economically and ecologically vulnerable regions (Balbus and Malina 2009; Cook et al. 2018;

✉ Qingyun Duan
qyduan@hhu.edu.cn

1 State Key Laboratory of Hydrology-Water Resources and Hydraulic Engineering, Hohai University, Nanjing, China

2 Department of Hydrology and Water Resources, Hohai University, Nanjing, China

3 CMA-HHU Joint Laboratory for Hydrometeorological Studies, Hohai University, Nanjing, China

4 State Key Laboratory of Earth Surface Processes and Resource Ecology, Faculty of Geographical Science, Beijing Normal University, Beijing, China

5 Yangtze Institute for Conservation and Development, Hohai University, Nanjing, China

Published online: 07 June 2022

Hirabayashi et al. 2013; Woolway et al. 2021). Tibet Plateau is recognized as the Third Pole of earth since its average elevation is above 4000 m (Zhao and Wu 2019). Pan-Third Pole (PTP) extends Third Pole to the southeast and northwest, covering Qinghai-Tibet Plateau, Pamirs, Hindu Kush and surrounding mountain ranges and origins a couple of large rivers such as Yangtze River, Yellow River and Lancang-Mekong River which provide water supply for millions of people downstream. In recent years, the northwestern part of China and its surrounding regions have experienced warmer and wetter climate and accelerated warming put great retreats to glacier, snow cover and permafrost in PTP, which are critical forms of water storage and determine the character of the hydrology, ecology, and biogeochemistry of the region (Du et al. 2019; Feng et al. 2021). On the other hand, the climate variability of PTP also has significant feedbacks on regional and continental scale climatology. Therefore, it is of vital importance to understand how long the "warm and wet" climate of PTP region will last and its impact on large scale climate change.

Global Climate Model (GCM) is a vital tool for projecting future changes in climate. Considering a large number of GCMs worldwide, the World Climate Research Program (WCRP) organizes regular international projects to intercompare these models known as Coupled Model Inter-comparison Projects-CMIPs) (Dufresne et al. 2013). The state-of-the-art CMIP experiment results are available as CMIP6 ensemble and it provides main evidence for the sixth IPCC assessment report (AR6). Compared with CMIP5, CMIP6 GCMs have shown significant improvements in spatial resolution, physical parameterizations and inclusion of additional earth system processes such as nutrient limitations on the terrestrial carbon cycle and ice sheets (Eyring et al. 2016). However, dynamic model simulation outputs are subject to uncertainty since models are different with respect to their structures, parameters, inputs and boundary conditions (Li et al. 2021; Liu et al. 2019; Mustafa et al. 2020; Yin and Tsai 2018). Instead of relying on the results of one specific model, extracting information from the model simulation ensemble has higher reliability, which indicates the model has higher chance to perform well under different conditions (Duan et al. 2007; Liu and Merwade 2019).

Bayesian model averaging (BMA) is a statistical approach to combine estimations from individual models and produce the reliable prediction based on weighted average (Raftery et al. 1997, 2005). The weight of a member is determined by its prediction skill in the training period. One benefit of BMA is that this approach not only provides the deterministic model weighted average prediction, but also provides an associated probability distribution which can reflect the prediction uncertainty. Previous studies indicated that although BMA prediction may not always perform the best, it typically behaves better than most individual models and ensemble mean (Liu and Merwade 2018; Yan et al. 2020). Since one single model performs well for one specific location and time period may not work equally well for another, given the reference information is lacking for future periods and ungauged locations, BMA prediction is more reliable than single model prediction.

Despite BMA has shown its advantages in various fields, it has seldom been applied for CMIP6 to investigate the variability of "warm and wet" condition for the future under complex system which is affected by westerlies and monsoons as well as various landforms (Eriș and Ulaşan 2013; Jiang et al. 2012; Massoud et al. 2020; Yin et al. 2021). Additionally, there is few study that creates the mixed distribution from multi-Gauging distributions. In this study, annual temperature and precipitation predictions from 16 CMIP6 models are trained with Climate Research Unit (CRU) historical observations through BMA approach to obtain the model weights and the weights are further applied to future under four different emission scenarios. We evaluated the BMA predictions of six 30-year mean climatology for both historical and future periods respectively to understand: (1) how CMIP6 models perform in capturing the spatio-temoral variations of historical annual temperature and precipitation climatology in PTP region; (2) whether or not and to what degree PTP will experience warmer and wetter climate in the future given different emission scenarios; (3) how much uncertainty is associated with the BMA consensus prediction of future climatology. The novel contribution of this study is that we investigate the performances of various CMIP6 models in the westerlies and monsoon synergistic affected region, which also has a range of landforms. This will provide useful information for future GCM model structure reformation and improvement under complexed climatological and geographical conditions. The persistence and trends of warmer and wetter conditions in PTP region is also investigated through BMA under various emission scenarios and this is critical for the snow, ice and frozen soil in PTP. Besides, the Bayesian-Gauging prediction distribution is constructed for this region to evaluate the uncertainty range. Findings from this study will provide constructive information for climate model developers and policy makers.

2 Study area and data

2.1 Study area

The Tibetan Plateau is named the Third Pole of earth after the North Pole and the South Pole since it has an average elevation of over 4000 m and contains the most spatially extensive highland in the world. PTP covers an area of more than 20 million square kilometers and provides the living environment for more than 3 billion people (Fan et al. 2021a).

It extends from the third pole to the northwest and southeast, covering Pamirs, Hindu Kush, Southeast Asian and the surrounding mountain ranges (Fig. 1). PTP origins a series of rivers including Yangtze River, Yellow River and Lancang-Mekong River and provide water supply for millions of people downstream (Yao et al. 2020). Cities in PTP have experienced rapid urbanization during the last few decades, which puts great stress on water demand and water security in the region (Immerzeel et al. 2010; Luan and Li 2021). In addition, PTP contains the largest cryospheric area outside the polar regions and this region has experienced unprecedented accelerated warming in the past decades which significantly retreats the glaciers, snow and frozen soil (Yao et al. 2012). The climate of PTP ranges from arid continental in the Central Asian to humid tropical in the Southeast Asian. Winter westerlies and summer Asian monsoon alternatively predominate the PTP regional. In this study, three subregions of PTP including Central Asian (CA, 35° N ~ 53° N, 44° E ~ 82° E), Tibetan Plateau (TP, 25° N ~ 45° N, 65° E ~ 105° E) and Southeast Asian (SEA, 8° N ~ 28° N, 90° E ~ 110° E) are studied respectively.

2.2 Data

2.2.1 CMIP6 climate data

Monthly temperature and precipitation predictions from the most recent Coupled Model Inter-comparison Project-Phase 6 (CMIP6) are used in this study to investigate the historical (1901–2010) and future (2015–2100) climate change in PTP. We applied 16 CMIP6 model (Table 1) predictions (download from https://esgf-node.llnl.gov/search/cmip6/) in this study. For future forecasts, simulations in CMIP6 are made under a set of combined Shared Socioeconomic Pathway (SSP) and Representative Concentration Pathways (RCPs). There are five SSPs which includes SSP1-sustainability: taking the green road; SSP2-middle of the road; SSP3-regional rivalry: a rocky road; SSP4-inequality: a road divided; and SSP5-fossil-fuelled development: taking the highway (Balbus and Malina 2009; Meinshausen et al. 2020; Van Vuuren et al. 2011). Each RCP value is corresponding to the level of radiative forcing in the unit of W/m^2. In this study, four combined SSP-RCP scenario outputs from "Tier1" simulations are used for future analysis (Table 2).

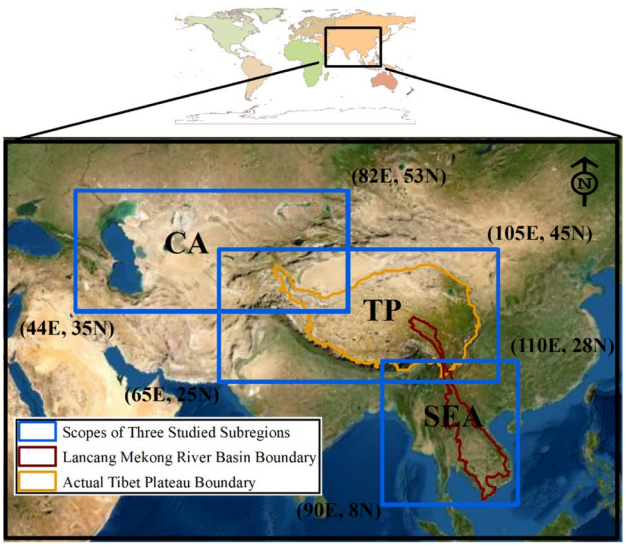

Fig. 1 Layout map of Pan Third Pole region. The scopes of Central Asian (CA), Tibet Plateau (TP) and Southeast Asian (SEA) used in this study are displayed in three blue boxes

2.2.2 CRU historical climate observations

Climatic Research Unit (CRU) is a widely used gauge-based gridded dataset developed by University of East Anglia (Harris et al. 2020). This dataset has 0.5° × 0.5° spatial resolution and monthly temporal resolution respectively. The CRU data is derived by interpolating monthly climate anomalies from extensive networks of weather station observations and extensively used by various studies as reference climate data for validating the model performances (Chen and Frauenfeld 2014; Lindvall and Svensson 2015; Liu et al. 2014; Nasrollahi et al. 2015; New et al. 2002). In this study, CRU TS v. 4.0.3 (download from https://crudata.uea.ac.uk/cru/data/hrg/cru_ts_4.03/) temperature and precipitation datasets are used as reference to evaluate CMIP6 historical prediction performance in PTP. Both the CMIP6 predictions and CRU observations are remapped to 1° × 1° spatial resolution using bilinear interpolation for model comparison and performance evaluation. It needs to be noted that bilinear interpolation might bring some uncertainty to the original CMIP6 predictions, however, various studies have adopted this approach in the resampling process and proved that its influence is not significant enough to alter the findings (Yang et al. 2021; Yue et al. 2021; Zhu and Yang 2020).

3 Methodology

3.1 Bayesian model averaging method

Bayesian model averaging approach is designed to combine multi-model predictions and provide a more reliable estimation by assigning weights to different models (Liu and Merwade 2018; Raftery et al. 2005). Assuming the probability density function (PDF) of variable y predicted by kth models is and the weight is w_k, the BMA predicted distribution can be estimated using Eq. (1). Since the multi-year mean annual

Table 1 List of CMIP6 Models and their resolutions

Model	Institution	Country/Region	Resolution (km)
BCC-CSM2-MR	Beijing Climate Center	China	320 × 160
CAMS-CSM1-0	Chinese Academy of Meteorological Sciences	China	320 × 160
CanESM5	Canadian Centre for Climate Modelling and Analysis, Environment and Climate Change Canada	Canada	128 × 64
CESM2	National Center for Atmospheric Research, Climate and Global Dynamics Laboratory	United States	288 × 192
CESM2-WACCM	National Center for Atmospheric Research, Climate and Global Dynamics Laboratory	United States	288 × 192
CNRM-CM6-1	National Centre for Meteorological Research	France	256 × 128
CNRM-ESM2-1	National Centre for Meteorological Research	France	256 × 128
EC-Earth3	EC-Earth Consortium	Europe	512 × 256
EC-Earth3-Veg	EC-Earth Consortium	Europe	512 × 256
FGOALS-g3	LASG, Institute of Atmospheric Physics, Chinese Academy of Sciences	China	180 × 80
GFDL-ESM4	National Oceanic and Atmospheric Administration, Geophysical Fluid Dynamics Laboratory	United States	288 × 180
IPSL-CM6A-LR	Institut Pierre Simon Laplace	France	144 × 143
MIROC6	JAMSTEC, AORI, NIES and R-CCS	Japan	256 × 128
MIROC-ES2L	JAMSTEC (Japan Agency for Marine-Earth Science and Technology), AORI (Atmosphere and Ocean Research Institute, The University of Tokyo), NIES (National Institute for Environmental Studies), and RCCS (RIKEN Center for Computational Science)	Japan	128 × 64
MRI-ESM2-0	Meteorological Research Institute	Japan	320 × 160
UKESM1-0-LL	Met Office Hadley Centre	United Kingdom	192 × 144

Table 2 Tier 1 combinations of SSP-RCP scenarios

SSP	RCP	Combination	Pathway property
1	2.6	SSP1-2.6	Sustainability and 2.6 W/m^2
2	4.5	SSP2-45	Middle of the road and 4.5 W/m^2
3	7.0	SSP3-70	Regional rivalry and 7.0 W/m^2
5	8.5	SSP5-85	Fossil-fueled development and 8.5 W/m^2

temperature and precipitation are used for analysis, the Gaussian distributions are assumed for both of them in this study.

$$\mathrm{p}\left(\mathrm{y}|M_1, M_2 \ldots, M_k\right) = \sum_{k=1}^{K} w_k \times p_k(y|M_k) \tag{1}$$

The model weights representing posterior probabilities of the models given target historical observations defined as $p_k(M_k|y_T)$. The maximum logarithmic likelihood function is applied to estimate the weight w_k, which is described in Eq. (2).

$$\mathrm{l}(\theta) = \sum_{s} \ln\left(\sum_{k=1}^{K} w_k p_k(y_s|M_{k,s})\right) \tag{2}$$

Equation (2) is difficult to solve analytically or numerically and thus an Expectation Maximization (EM) algorithm is used to find out the maximum likelihood (Liu and Merwade 2018; Vrugt and Robinson 2007). The details of EM method is shown in the "Appendix". The EM method produces the model weight $\mathrm{w_k}$ and we can calculate BMA consensus prediction using Eq. (3).

$$\mathrm{E}\left(\mathrm{y}|M_1, M_2 \ldots, M_k\right) = \sum_{i=1}^{K} w_k \times M_k \tag{3}$$

$$\sigma^2\left(\mathrm{y}|M_1, M_2 \ldots, M_k\right) = \sum_{i=1}^{K} w_k \times \left(\sum_{i=1}^{K} M_k - \sum_{i=1}^{K} w_k \times M_k\right)^2 + \sum_{i=1}^{K} w_k \times \sigma^2\left(y_T|M_k\right) \tag{4}$$

The associated total variances that are measures of the spread (or uncertainty) of the posterior PDFs given by Eq. (4). The first term on the right side of Eq. (4) is the inter-model contribution and the second term is intra-model contribution to the measure of overall uncertainty. A Monte Carlo sampling approach is applied to generate BMA consensus Gaussian mixture PDF and calculate the corresponding mean BMA prediction (Duan and Phillips 2010).

3.2 Evaluation of CMIP6 model performance in historical periods

In this study, we separate historical data into three 30-year periods to represent far history (1901–1930), middle history (1941–1970) and near history (1981–2010) respectively. Since the historical period we investigated ranges from 1901 to 2010 (110 years), there exist a 10-year gap between each two defined periods, but this won't affect their representation of model outputs for different time spans in history. The spatial distributions of bias of annual mean temperatures and annual total precipitation between model predictions (16 CMIP6 models and BMA) and corresponding CRU observations are calculated. Besides model prediction bias, the Taylor diagram is also applied to further evaluate the RMSD, correlation coefficient and standard deviation between model predictions and observations. The details of model bias and Taylor diagram are described in Sect. 3.4.

3.3 Assessment of BMA projected climatology for future periods

Similarly, three 30-year periods representing near future (2021–2050), middle future (2046–2075) and far future (2071–2100) are evaluated in this study. The defined periods are slightly overlapped since the future data only ranges from 2015 to 2100 (86 years) and we want to keep each period to be consistent with 30-year length for convenient comparison. Four future scenarios including SSP1-2.6, SSP2-4.5, SSP3-7.0 and SSP 5-8.5 are applied in this study to assess the future annual mean temperature and annual total precipitation. The spatial distribution of BMA prediction is calculated for each modeling scenario and the difference between predictions in each future period and baseline period (1981–2010) are investigated. In addition, the linear trends of annual mean temperature and annual total precipitation are also calculated for each future period and each modeling scenario respectively. The significance test of trend is performed and marked when increasing or decreasing rate is below the statistical threshold.

The Gaussian mixture PDFs of BMA consensus estimates are generated for each modeling scenario and period based on the Monte Carlo sampling technique with 10,000 sample times in this study (Duan and Phillips 2010). The mean value corresponds to 50% percentile of Gaussian mixture PDF is also calculated for annual mean temperature and annual total precipitation respectively. Moreover, the ensemble model predicted temperature and precipitation anomalies are also evaluated and compared with BMA prediction anomaly in this study. Both Gaussian mixture PDF of BMA prediction and

model ensemble anomaly declare the uncertainty associated with BMA consensus prediction.

3.4 Performance measures

3.4.1 Model bias

Bias is the difference between modelled and observed values. Previous studies have shown that the bias of predictions from GCMs can be the same order as observations, therefore, it is used to quantify the model performance in this study (Lyu et al. 2020; Tian and Dong 2020). Firstly, the bias of 30-year mean temperature and precipitation climatology values are derived from CMIP6 models and CRU for each grid respectively and this displays the spatial pattern of model performance in PTP region. Secondly, the 30-year mean values are further averaged along the longitude and latitude dimensions to obtain the regional averaged climatology values for CA, TP and SEA respectively (Eq. 5).

$$\text{Bias} = \overline{Model}_{t,lon,lat} - \overline{Observation}_{t,lon,lat} \quad (5)$$

3.4.2 Taylor diagram

Taylor diagram is commonly used to compare the relative merits of a collection of different models (Taylor 2001). Taylor diagram summarizes three statistics in one figure, horizontal and vertical axes show standard deviation, radial axis shows spatial correlation coefficient and concentric circle denotes centered RMSD. The values with correlation coefficient and the standard deviation are 1 and the RMSD is 0 yield the best match between observation and model simulation. The detailed equation of Taylor diagram is shown in the Appendix.

4 Results and discussion

4.1 CMIP6 model performance in historical periods

The spatial distributions of 30-year (1981–2010) mean climatology of annual temperatures and precipitation bias between models (16 CMIP6 models as well as BMA) and CRU observations over the PTP region are shown in Figs. 2 and 3 respectively. The last subfigure on the lower right side of figure shows the observed annual mean temperature or annual total precipitation with the corresponding color bar. Comparatively, another color bar shown in Figs. 2 or 3 is absolute model bias of annual temperature or precipitation. Generally, the observed annual mean temperature exhibits an increasing gradient from the north to south. Most models underestimate annual mean temperature for the high elevation TP region except for CESM2 and CESM2-WACCM models which slightly overestimate temperature. Similarly, most models underestimate annual mean temperature

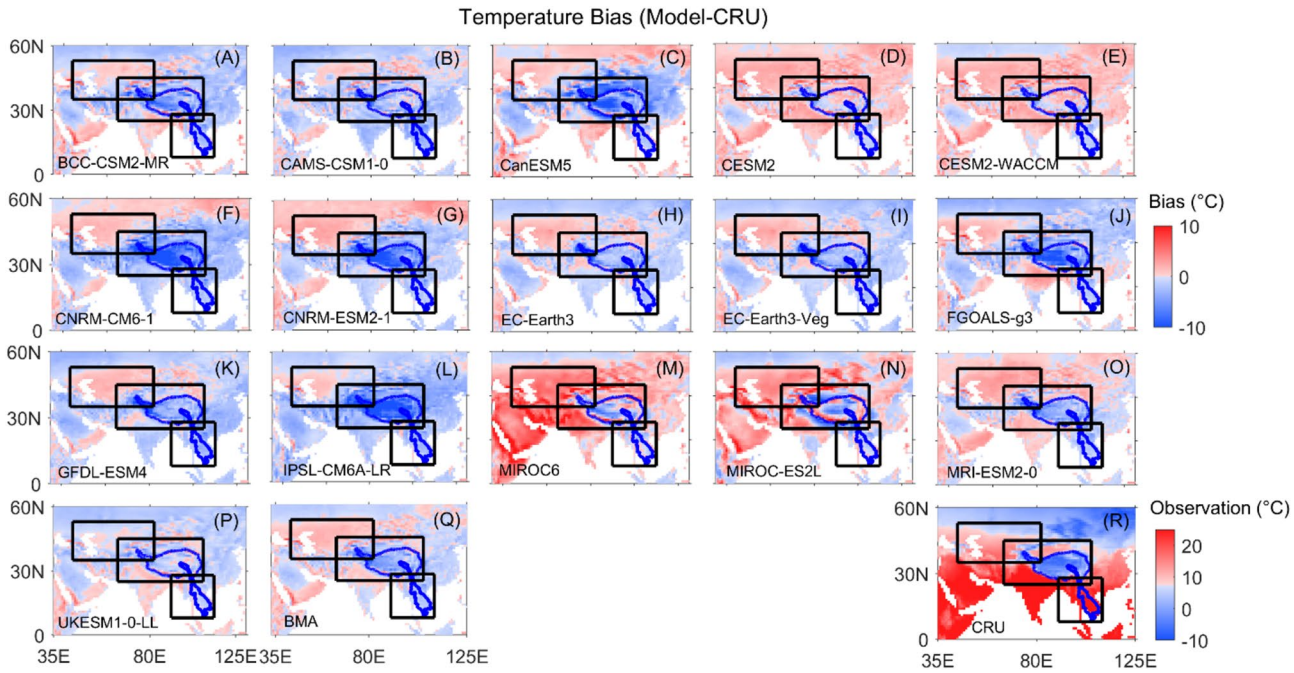

Fig. 2 Spatial distributions of annual mean temperatures bias between 16 CMIP6 models as well as BMA and CRU observations over the PTP region for 1981–2010

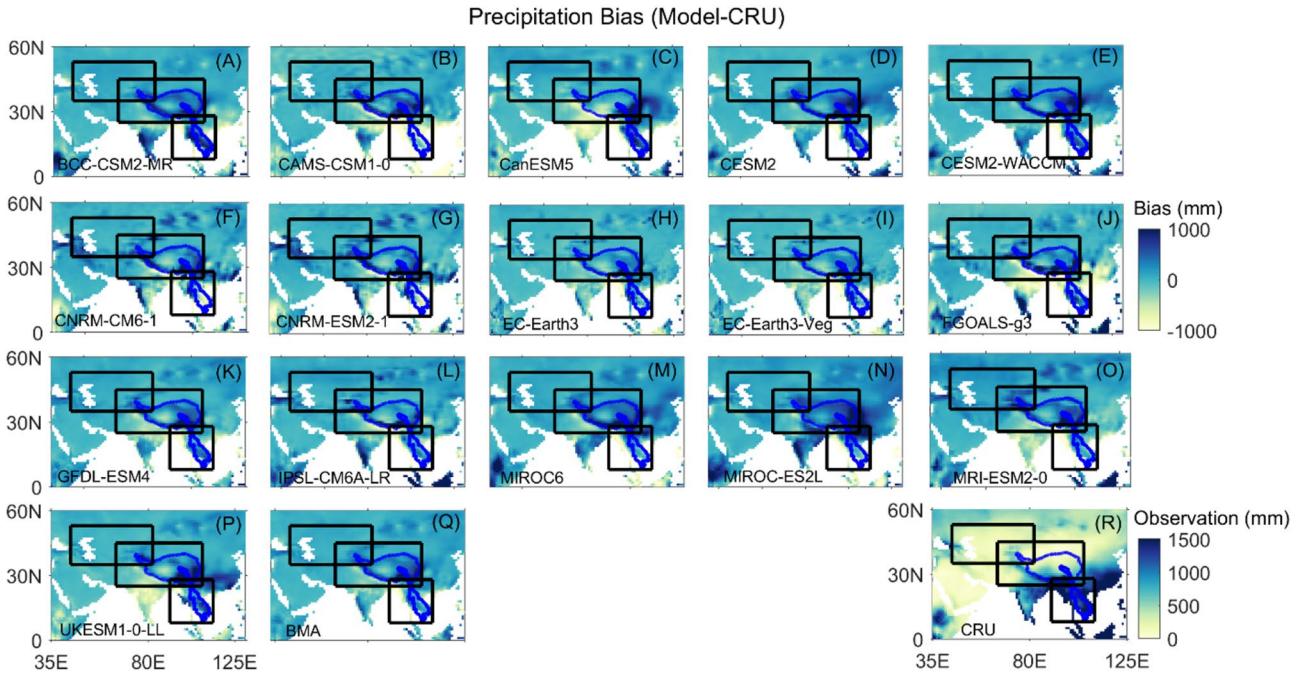

Fig. 3 Spatial distributions of annual total precipitation bias between 16 CMIP6 models as well as BMA and CRU observations over the PTP region for 1981–2010

(underestimate 0.5–1.8 °C) for SEA whereas overestimate for CA (0–4 °C). The SEA and southeast part of TP have larger annual total precipitation around 1500 mm, which are strongly related to south Asian monsoon. Comparatively, the annual total precipitation for northwest part of TP and CA is less than 300 mm. All models overestimate annual total precipitation for CA and TP whereas significant model differences exist for SEA. For instance, UKESM1-0-LL, MIROC6, CESM2 and CESM2-WACCM models overestimate annual total precipitation for about 200 mm for SEA whereas CAMS-CSM1-0 and FGOALS-g3 models underestimate annual total precipitation close to 400 mm. Overall, the bias distribution of BMA prediction shows better performance than most individual models. Moreover, we also conducted seasonal temperature and precipitation bias analysis for the PTP regions (see Figure S1–S4 in the supplementary materials). In general, it shows bias patterns are very different between JJA and DJF. Temperature has positive bias in JJA for most mid to low latitude regions (except high elevation part of TP) whereas bias turns to be negative for DJF for these regions. Comparatively, precipitation bias is higher for JJA in monsoon affected southern TP and SEA regions whereas it is lower for DJF. This reflects that current CMIP6 models still have certain capacity to improve their ability in capturing temperature more accurately in high elevation mountainous regions and precipitation more precisely in monsoon affected regions.

Figures 4 and 5 show the bias of regional averaged annual mean temperature and annual total precipitation climatology for the far historical period (1901–1930), middle historical period (1941–1970) and near historical period (1981–2010) respectively. As shown in figures, overall bias displays similar patterns (overestimate or underestimate) among different models except annual temperature in CA and annual total precipitation in SEA. In addition, Fig. 4 shows the CA region has the largest temperature difference between the high latitude and low latitude areas. The annual mean temperature increase for CA is about 1.2 °C during the past century whereas it is 0.6 and 0.3 °C for TP and SEA respectively. Comparatively, Fig. 5 shows that annual total precipitation has been slightly increased for CA (from 277 to 291 mm) during 1901–2010 whereas there is no monotonously change for TP and SEA. Although models behave distinctly, most models underestimate annual mean temperature for TP (1 ~ 5 °C) and SEA (0.2 ~ 1.8 °C) and overestimate annual total precipitation for CA (10 ~ 200 mm) and TP (30 ~ 350 mm). BMA performs the best regarding annual mean temperature prediction for TP and annual total precipitation for SEA since the regional averaged bias is smallest. For other regions, BMA prediction is also reliable and performs better than most individual CMIP6 models.

Figures 4 and 5 only evaluate the model and BMA performances based on the regional averaged bias, which is not enough to quantify the overall model behavior. Figures 6 and 7 show the Taylor diagrams for assessing the performance

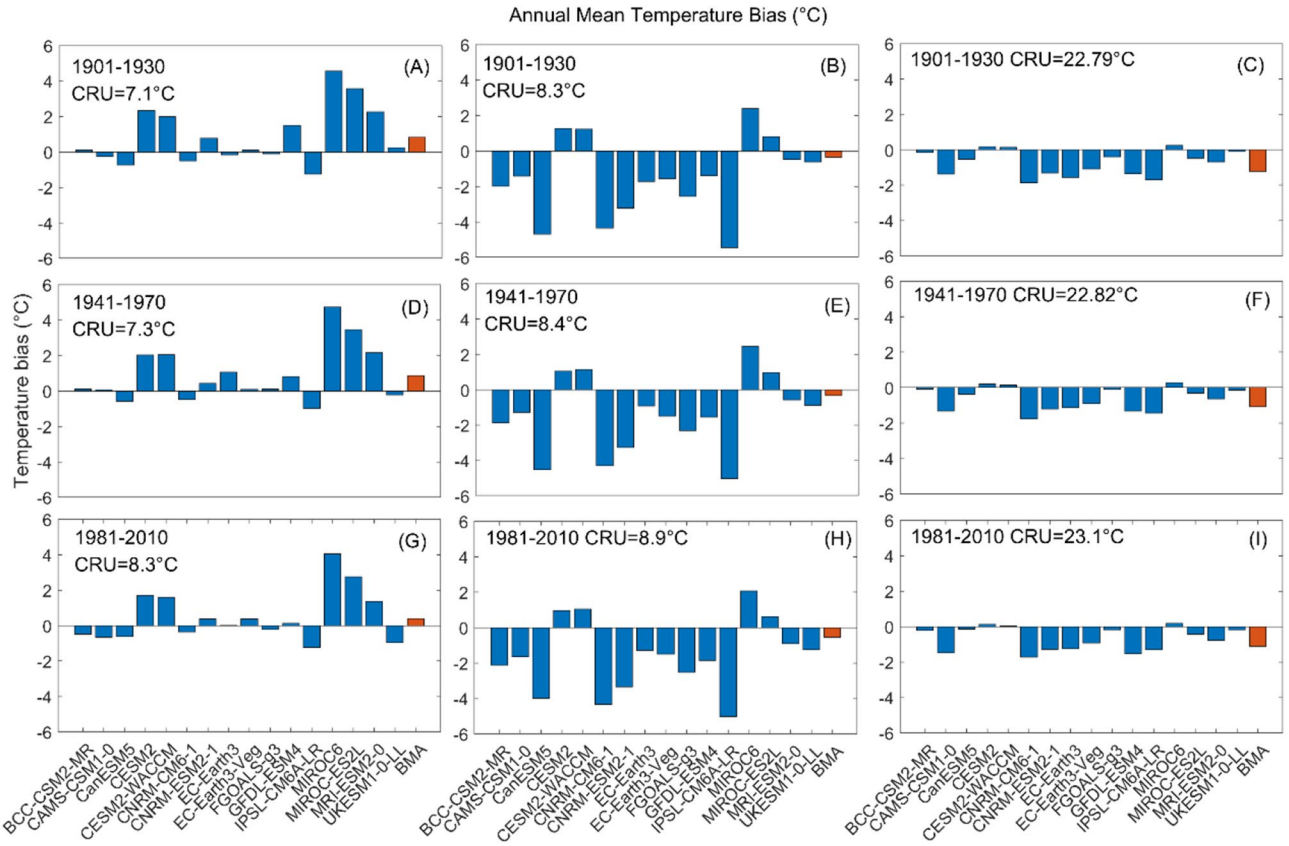

Fig. 4 Regional averaged CMIP6 models (blue bars) and BMA (red bar) annual mean temperature bias for the far historical period (1901–1930, first row), middle historical period (1941–1970, second row) and near historical period (1981–2010, third row). The first to third column corresponds to CA, TP and SEA respectively

of models in simulating the spatial pattern of annual mean temperature and annual total precipitation climatology for CA, TP and SEA respectively. Figure 6 indicates that all 16 CMIP6 models and BMA annual mean temperature predictions have great agreement with CRU observations. The correlation coefficients are 0.8–0.95 for CA, 0.94–0.96 for TP and 0.9–0.97 for SEA respectively among different models. Comparatively, Fig. 7 illustrates that CMIP6 model historical annual precipitation predictions are also in line with CRU observations, however the correlation coefficients (0.6–0.8 for CA, 0.68–0.86 for TP and −0.1 to 0.4 for SEA) are slightly worse compared with those for annual temperature climatology. Similarly, RMSDs and STDs are smaller for annual mean temperature predictions, both of which are 0.3–0.6 for three regions in PTP. Comparatively, RMSDs of annual total precipitation are 0.5–1.5 for PTP and STDs are 0.7–1.3 for CA and TP and 0-0.5 for SEA. It can be seen from Figs. 2, 3, 6 and 7 that CMIP6 models generally captures temperature very well for monsoon and westerlies synergistic affected region with various landform types. However, models behave differently in precipitation predictions. Current models simulate precipitation very well for mountainous regions such as northwest part of Tibet Plateau and east part of CA, but most CMIP6 models could not reproduce precipitation well enough for SEA region, which suggests that future improvement need to be made for GCM models to better represent precipitation for low latitude, monsoon affected area.

As we mentioned before, BMA is a weighted average prediction and the weight is obtained based on the posterior distribution given historical observations and it does not guarantee that BMA will be better than any model prediction in the ensemble. Figures 6 and 7 have proved this and indicate that although models perform differently among regions and periods, BMA prediction is always one of the best performed models in the ensemble (as can be found from the distances between model points to the reference point). This points out that BMA prediction is generally more reliable than individual models given the best individual model is unknown for future prediction under various regions and periods and BMA consensus prediction is a robust choice for future projections and analysis.

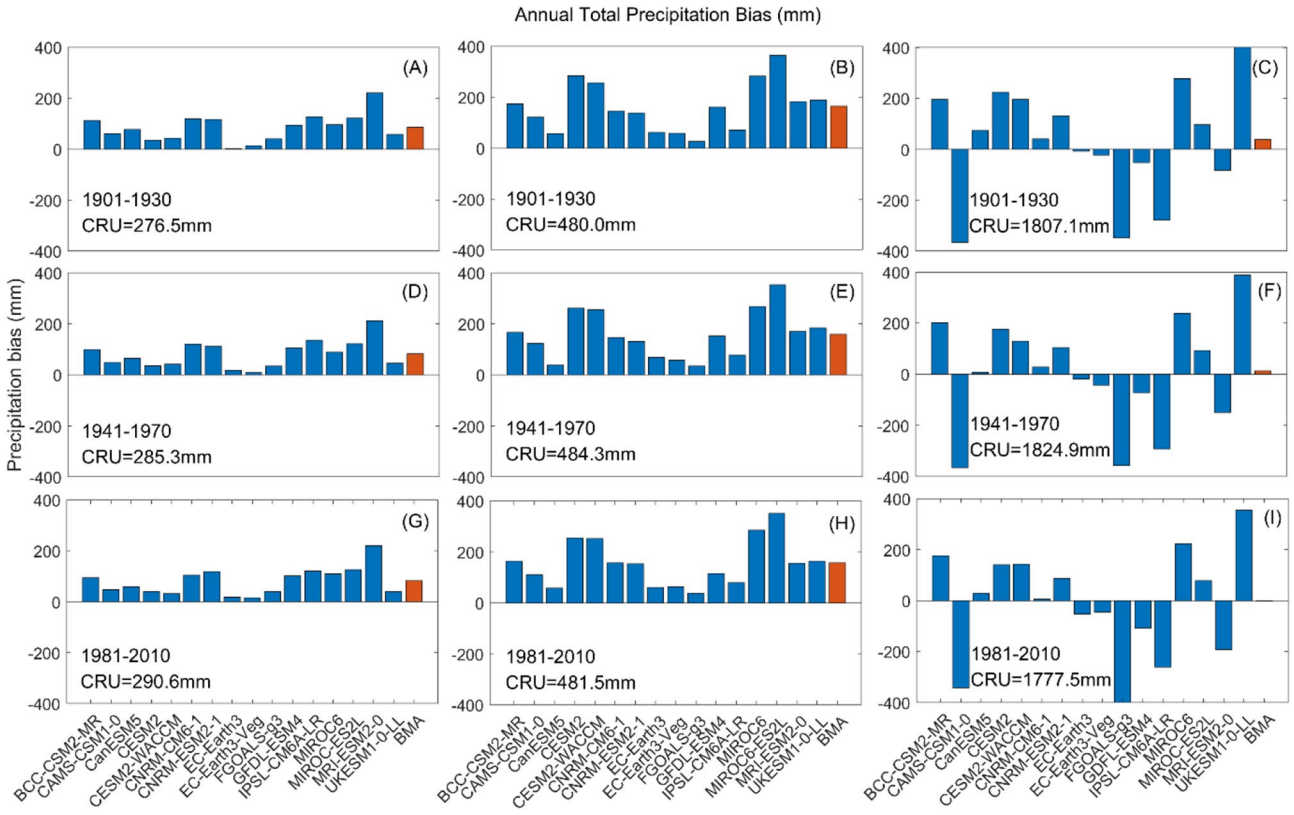

Fig. 5 Regional averaged CMIP6 models (blue bars) and BMA (red bar) annual total precipitation bias for the far historical period (1901–1930, first row), middle historical period (1941–1970, second row) and near historical period (1981–2010, third row). The first to third column corresponds to CA, TP and SEA respectively

4.2 BMA projected temperature and precipitation change for the future

Figures 8 and 9 show the BMA projected 30-year mean temperature and precipitation climatology change between near future, middle future, far future and the baseline period (1981–2010) under SSP1-2.6, SSP2-4.5, SSP3-7.0 and SSP5-8.5 scenarios for PTP region. Figure 8 states that temperature is projected to continuously increase till the end of the century under all four scenarios. In addition, the high latitude mountainous region has stronger temperature increase than the low latitude costal and monsoon affected region. For instance, SEA is projected to increase 1–2 °C in far future (2071–2100) whereas CA is projected to increase 2–3 °C under SSP1-2.6 scenario. Figure 9 indicates that precipitation is projected to increase in PTP for the future as well. However, on the contrary, monsoon affected SEA and southern part of TP have stronger precipitation increase than CA. Additionally, Figs. 8 and 9 also indicate that both temperature and precipitation increase become heavier under more severe SSP scenarios.

Figures 10 and 11 illustrate the linear trends of BMA projected 30-year temperature and precipitation climatology under SSP1-2.6, SSP2-4.5, SSP3-7.0 and SSP5-8.5 scenarios for the near future, middle future and far future respectively. The statistical significance tests are performed and those grids pass the significance test ($\alpha = 0.05$) are marked with black dots. Overall, Fig. 10 indicates that temperature in PTP region has an increasing trend for the future periods. The increasing rate is projected to be 0.2 ~ 0.8 °C/decade under SSP1-2.6, SSP2-4.5 and SSP3-7.0 scenarios and it could reach above 1 °C/decade under SSP5-8.5 scenario especially for the high latitude CA and TP regions. In addition, the increasing trend of 30-year mean temperature climatology is predicted to slightly decreases from near future to far future under SSP 1-2.6 and SSP2-4.5 scenarios (i.e. increasing trend decreases from 0.5 to 0.2 for TP region) whereas it is projected to continuously increase under SSP3-7.0 and SSP5-8.5 scenarios. This implies that the rate of global warming can be alleviated in the future if we reduce the greenhouse gas (GHG) emission and apply the sustainable development strategy. On the contrary, without proper supervision on socio-economic development and strict control on GHG emission, the temperature of PTP will increase quicker in the future which will have irreversible

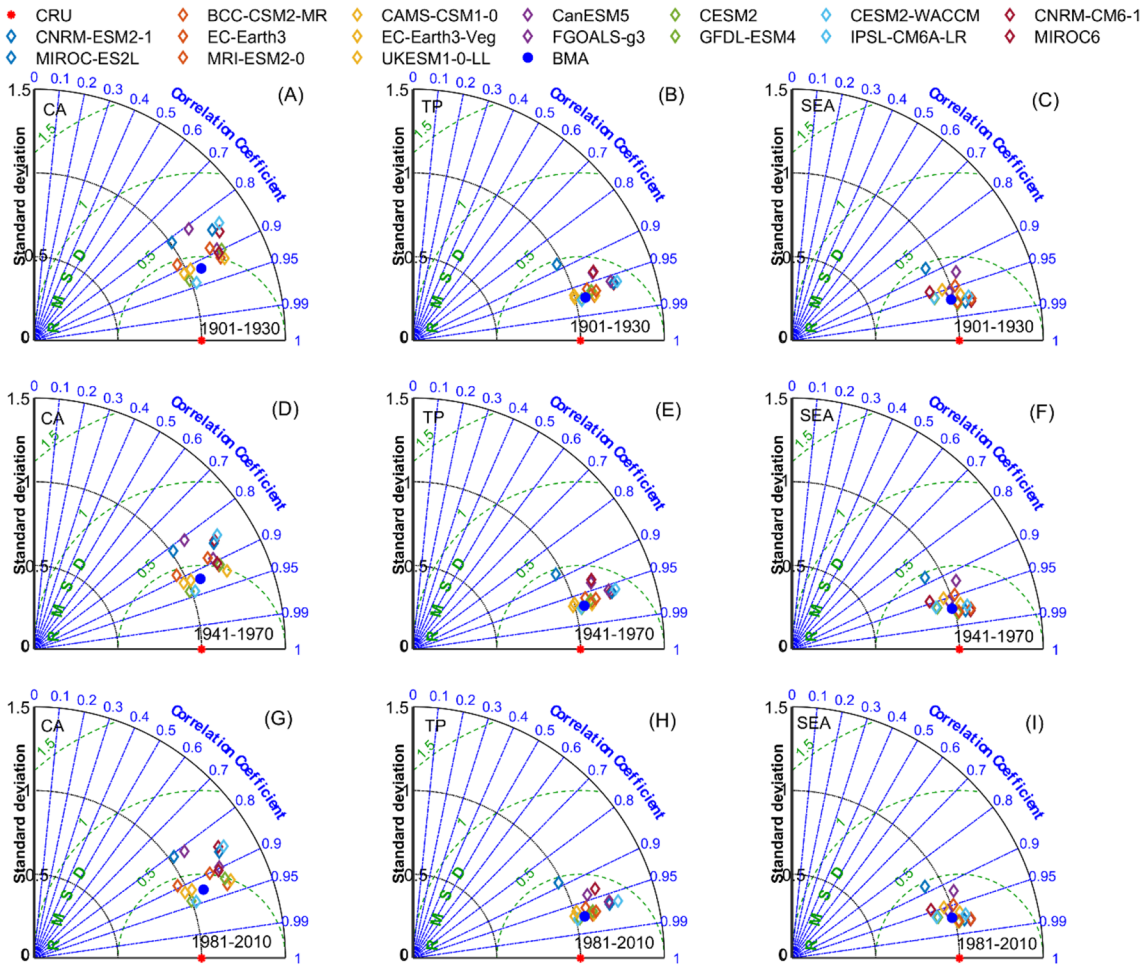

Fig. 6 Taylor diagram of climatological annual mean temperature generated from 16 CMIP6 models, BMA and CRU in the PTP region for far historical period (1901–1930), middle historical period (1941–1970) and near historical period (1981–2010). The first to third column corresponds to CA, TP and SEA respectively

impact on PTP environment. In general, the high latitude CA region has higher increasing trend compared with lower latitude TP and SEA regions and the increasing trend all pass significance test except when the SSP1-2.6 scenario is applied for the middle to far future. Figure 11 demonstrates that 30-year precipitation is also projected to have an increasing trend for PTP region in the future. The trend is stronger for the SEA and southeast part of TP regions which could be more than 20 mm/decade. The trend becomes stronger as prediction scenario changing from SSP1-2.6 to SSP5-8.5. Comparatively, the increase rate for the rest part of TP and CA is less than 10 mm/decade. Different from temperature trend, generally most parts of CA and SEA did not pass significance tests for precipitation trend under all four scenarios. However, precipitation trends in large portion of TP pass the significance test under SSP3-7.0 and SSP5-8.5 scenarios.

4.3 The uncertainty associated with BMA forecasts

Figure 12 demonstrates the BMA predictions of annual mean temperature and annual total precipitation anomaly as well as the 5th percentile to 95th percentile prediction ranges of CMIP6 anomaly ensemble for CA, TP and SEA respectively. Results indicate that BMA prediction of temperature anomaly has increased in the past century and will continue increase from 0.012 to 0.078 °C/year for CA, 0.012 to 0.074 °C/year for TP and 0.010 to 0.054 °C/year for SEA under SSP1-2.6 to SSP5-8.5 scenarios. Considering the 90% confidence interval, the range of temperature anomaly is projected to increase to 0 ~ 10 °C for CA, -3 ~ 8 °C for TP and − 1 ~ 7 °C for SEA till the end of the century under different scenarios. Comparatively, the precipitation anomaly is relatively stable for the historical period whereas the BMA predictions show slightly increasing trend for the future for

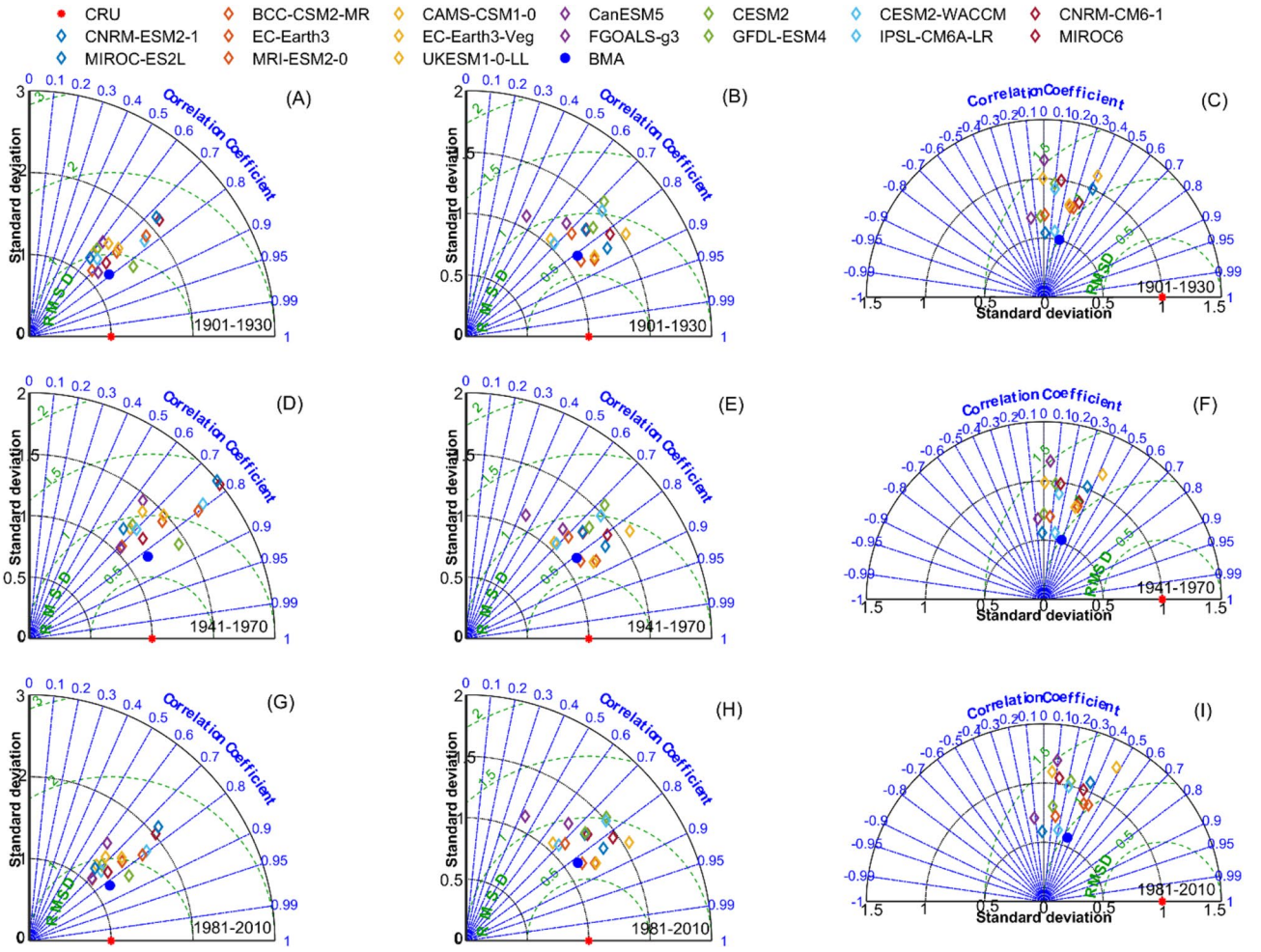

Fig. 7 Taylor diagram of climatological annual total precipitation generated from 16 CMIP6 models, BMA and CRU in the PTP region for far historical period (1901–1930), middle historical period (1941–1970) and near historical period (1981–2010). The first to third column corresponds to CA, TP and SEA respectively

all three regions. Figure 12D shows precipitation anomaly is projected to increase the most in TP (from 180 to 300 mm under SSP5-8.5 scenario) whereas Fig. 12B indicates precipitation anomaly is projected to increase less in CA (from 80 to 110 mm) till the end of the century. This might be because TP has high elevation difference and affected by India monsoon as well as westerlies and this makes TP more sensitive to precipitation variation. Comparatively, the landform is relatively uniform and monsoon have less influence on CA region, thus the corresponding precipitation change is less. The range of precipitation anomaly is projected to be 0–300 mm for CA, 50–500 mm for TP and − 400 to 600 mm for SEA respectively.

Figures 13 and 14 show the Probability Density Function (PDF) of BMA prediction, which is the weighted combination of normal distribution from individual model members. Instead of showing only the mean predictions which are summarized in Table 3, PDF also demonstrates the uncertainty (BMA prediction ranges) associated with BMA consensus predictions. Figure 13 indicates that CA have higher temperature increase for future compared with TP and SEA regions as the peak of annual mean temperature PDFs shift significantly to the right side from historical baseline period to far future. For instance, the temperature ranges from 2 ~ 15 °C for CA (BMA mean 8.5 °C, Table 3) and 15 ~ 26 °C for SEA (BMA mean 19.8 °C) for historical baseline period. While for the far future, the range of annual mean temperature is projected to increase to 6 ~ 23 °C for CA (BMA mean 14.6 °C) and 19 ~ 33 °C for SEA (BMA mean 24.1 °C) respectively. In addition, the amount of temperature increase becomes more from SSP1-2.6 to SSP5.85 scenarios for all three regions. Figure 14 shows that the BMA Gaussian mixture PDF of annual total precipitation are generally the same as historical period for the future. However, under severe scenarios (i.e. SSP 5-8.5), there is a slightly increasing trend for the future.

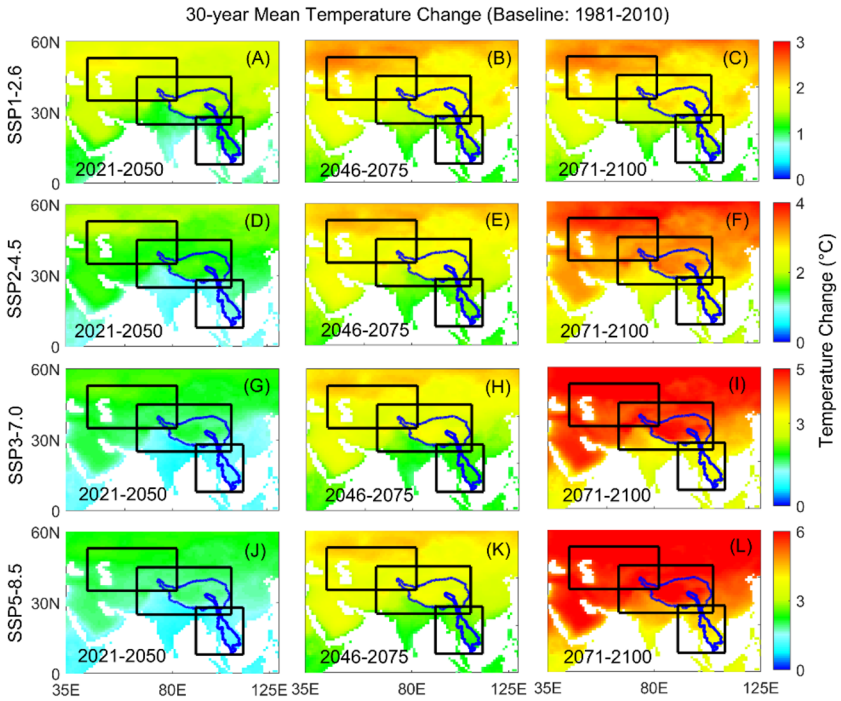

Fig. 8 BMA projected 30-year mean temperature change (baseline period:1981–2010) under SSP1-2.6 (**A**–**C**), SSP2-4.5 (**D**–**F**), SSP3-7.0 (**G**–**I**) and SSP5-8.5 (**J**–**L**) scenarios respectively for near future (2021–2050), middle future (2046–2075) and far future (2071–2100)

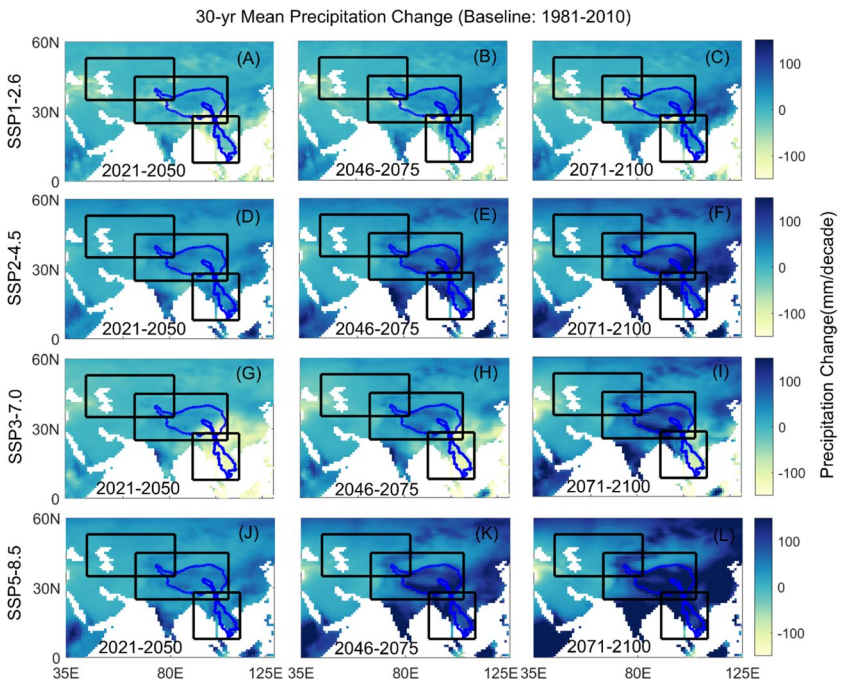

Fig. 9 BMA projected 30-year mean precipitation change (baseline period:1981–2010) under SSP1-2.6 (**A**–**C**), SSP2-4.5 (**D**–**F**), SSP3-7.0 (**G**–**I**) and SSP5-8.5 (**J**–**L**) scenarios respectively for near future (2021–2050), middle future (2046–2075) and far future (2071–2100)

The BMA mean annual total precipitation are 359, 601 and 1582 mm for CA, TP and SEA respectively for the historical baseline period and under SSP5-8.5 scenario, these become 391, 711 and 1761 mm for the far future (Table 3). Moreover, uncertainty range associated with BMA annual total precipitation prediction is higher for SEA region (0–3800 mm).

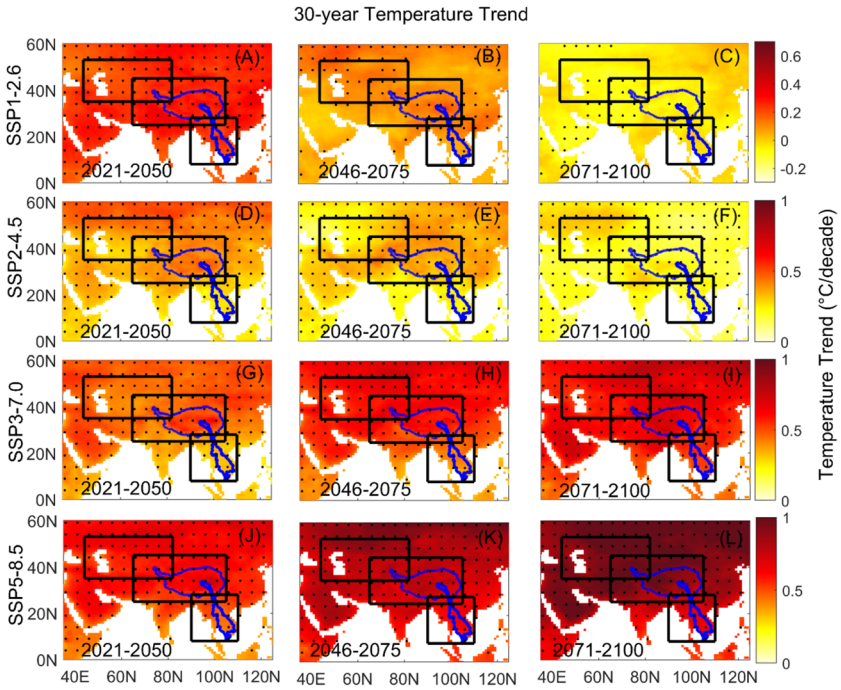

Fig. 10 BMA projected 30-year temperature trend under SSP1-2.6 (**A**–**C**), SSP2-4.5 (**D**–**F**), SSP3-7.0 (**G**–**I**) and SSP5-8.5 (**J**–**L**) scenarios respectively for near future (2021–2050), middle future (2046–2075) and far future (2071–2100). Black dots denote the trends pass the statistical significance test ($\alpha = 0.05$)

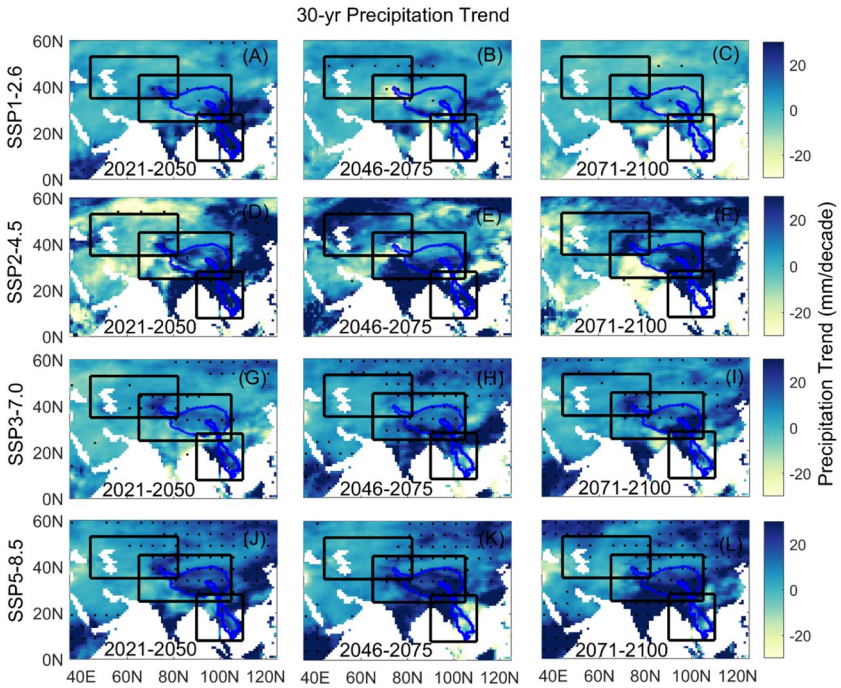

Fig. 11 BMA projected 30-year precipitation trend under SSP1-2.6 (**A**–**C**), SSP2-4.5 (**D**–**F**), SSP3-7.0 (**G**–**I**) and SSP5-8.5 (**J**–**L**) scenarios respectively for near future (2021–2050), middle future (2046–2075) and far future (2071–2100). Black dots denote the trends pass the statistical significance test ($\alpha = 0.05$)

5 Conclusions

This study evaluates the historical performance of temperature and precipitation climatology of 16 CMIP6 models with CRU observations in capturing spatio-temporal variations over westerlies and monsoon synergistic affected PTP region. BMA predictions are further projected to the near future (2021–2050), middle future (2046–2075) and far future (2071–2100) under SSP1-2.6, SSP2-4.5, SSP3-7.0 and SSP5-8.5 respectively to investigate the persistence of "warmer and wetter" conditions in the future. Moreover, the Bayesian-Gaussian mixture PDFs are generated for Central Asian, Tibet Plateau and Southeast Asia respectively to evaluate the uncertainty associated with the

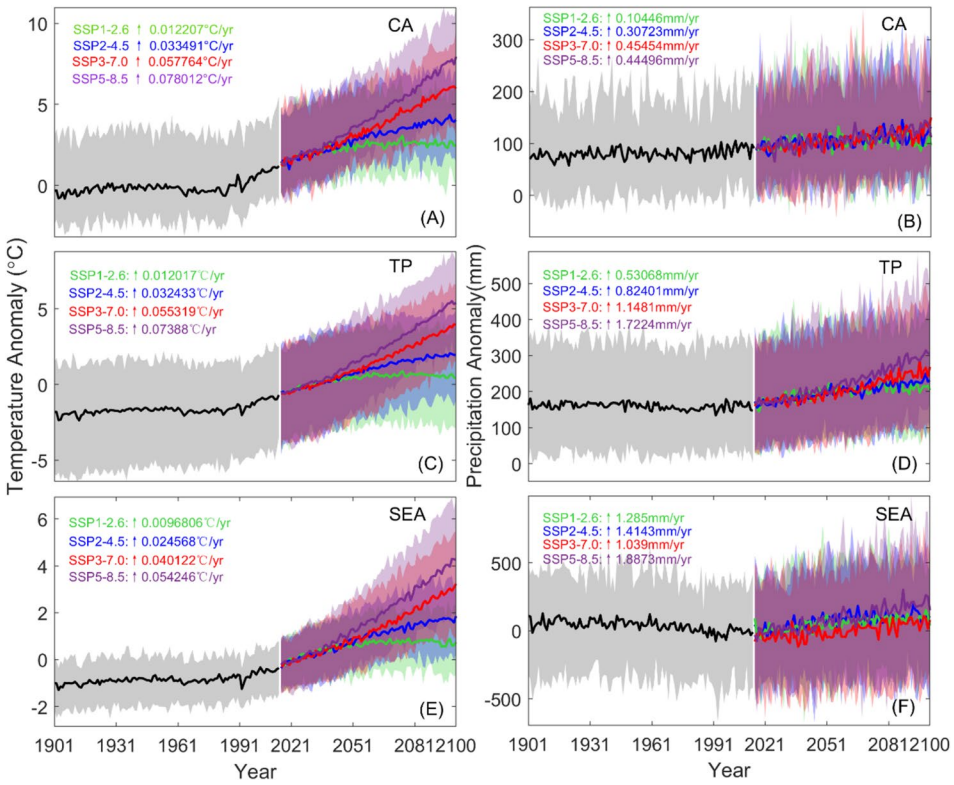

Fig. 12 Time series of anomaly in annual mean temperature and annual total precipitation over CA, TP and SEA during 1901–2100 (baseline period: 1981–2010). The shaded areas are the spreads from the 5th to the 95th percentiles of the annual mean temperature and annual total precipitation. The solid lines in the middle are BMA consensus predictions for historical period and future under different scenarios respectively

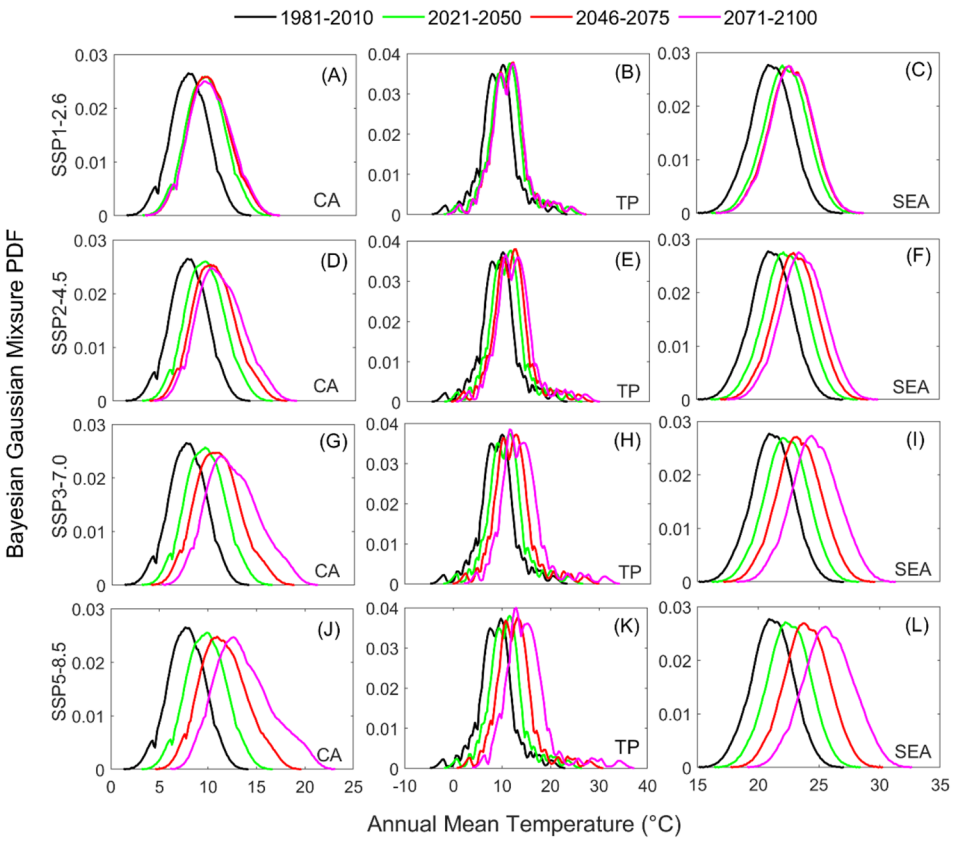

Fig. 13 Bayesian Gaussian mixture probability density function of annual mean temperature under SSP1-2.6 (**A**–**C**), SSP2-4.5 (**D**–**F**), SSP3-7.0 (**G**–**I**) and SSP5-8.5 (**J**–**L**) scenarios for CA, TP and SEA during historical baseline period (1981–2010), near future (2021–2050), middle future (2046–2075) and far future (2071–2100)

Table 3 Mean of BMA consensus predictions for annual mean temperature and annual total precipitation under SSP1-2.6, SSP2-4.5, SSP3-7.0 and SSP5-8.5 scenarios for CA, TP and SEA during historical baseline period (1981–2010), near future (2021–2050), middle future (2046–2075) and far future (2071–2100)

T_{annual_mean} (°C)	Scenario	Period	CA	TP	SEA
	Historical	1981–2010	8.5	8.4	19.8
	SSP126	2021–2050	10.2	9.9	20.9
	SSP126	2046–2075	10.6	10.3	21.3
	SSP126	2071–2100	10.7	10.3	21.3
	SSP245	2021–2050	10.3	9.9	20.8
	SSP245	2046–2075	11.2	10.8	21.6
	SSP245	2071–2100	11.9	11.4	22.2
	SSP370	2021–2050	10.4	9.9	20.9
	SSP370	2046–2075	11.7	11.1	21.8
	SSP370	2071–2100	13.4	12.7	23.1
	SSP585	2021–2050	10.6	10.2	21.1
	SSP585	2046–2075	12.5	11.9	22.4
	SSP585	2071–2100	14.6	13.9	24.1
P_{annual_total} (mm)	Historical	1981–2010	359	602	1582
	SSP126	2021–2050	357	594	1517
	SSP126	2046–2075	360	609	1574
	SSP126	2071–2100	362	614	1584
	SSP245	2021–2050	369	619	1603
	SSP245	2046–2075	374	640	1644
	SSP245	2071–2100	384	657	1666
	SSP370	2021–2050	347	589	1473
	SSP370	2046–2075	355	612	1511
	SSP370	2071–2100	366	645	1560
	SSP585	2021–2050	369	629	1607
	SSP585	2046–2075	379	663	1674
	SSP585	2071–2100	391	711	1761

BMA predictions. Specifically, the following conclusions are drawn from this study:

1. Most CMIP6 models underestimate historical annual mean temperature about 1 ~ 5 °C for the TP region and 0.2–1.8 °C for SEA whereas overestimate 0 ~ 4 °C for CA. Comparatively, most models overestimate precipitation around 0 ~ 100 mm (0–36%) for CA and about 30–350 mm (6–73%) for TP. Large discrepancy (− 400 ~ 400 mm bias, around − 22~22%) exist among models in simulating precipitation for SEA region. This demonstrates that CMIP6 models have relatively worse performance in southeast Asian region and current model structure and physics might not capture precipitation dynamics well enough for the low latitude, monsoon-affected SEA regions. Seasonal bias analysis results indicate that bias patterns vary significantly between JJA and DJF. Models need to improve their ability in capturing accurate temperature in high altitude mountainous regions.
2. BMA predictions are always the best or among one of the best performed models in simulating the spatial pattern of annual temperature and precipitation climatology for all three regions. This suggests that BMA is a robust and reliable estimation which is proper for analyzing future climatology.
3. The annual mean temperature of PTP region has continuously increasing trend till the end of this century under SSP2-4.5, SSP3-7.0 and SSP5-8.5 scenarios. This indicates that PTP region will be likely to experience accelerated warmer and wetter climate in the future. The high latitude mountainous CA and northwest part of TP regions have higher temperature increase than the relatively lower latitude, monsoon affected SEA regions. As scenario becomes more severe, the level of annual mean temperature increase becomes higher and annual temperature is projected to increase more than 5 °C for CA and TP under SSP5-8.5 scenarios by the end of the century. Comparatively, annual total precipitation is projected to increase slightly under SSP3-7.0 and SSP5-8.5 scenarios for the future and the increase is more obvious for monsoon affected SEA region.
4. The annual mean temperature has an increasing trend for the future and almost all the grids pass the statistical significance test except SSP1-2.6 scenario. The trend is 0.2 ~ 0.8 °C/decade under SSP1-2.6, SSP2-4.5 and SSP3-7.0 scenarios whereas it reach above 1 °C/decade under SSP5-8.5 scenario. This indicates that anthropogenic contributions of greenhouse gas emissions and socio-economic development could significantly affect the warming rate and the warming could slow down if we apply the sustainable development strategy. Precipitation is also projected to have a slightly increasing trend for PTP region for the future. The trend is stronger for the SEA and southeast part of TP regions which could be more than 20 mm/decade. However, most parts of CA and SEA did not pass statistical significance test for annual total precipitation trend.
5. The temperature anomaly is projected to increase to 0 ~ 10 °C for CA, -3 ~ 8 °C for TP and − 1 ~ 7 °C for SEA till the end of the century based on 90% confidence interval of model prediction ensemble. Comparatively, precipitation anomaly is projected to be 0–300 mm (0 ~ 103%), 50–500 mm (10 ~ 104%) and − 400–600 mm (− 22 ~ 34%) till the end of century for CA, TP and SEA regions. In addition, Bayesian-Gaussian mixture PDF indicates that the uncertainty associated with BMA temperature prediction is larger for high latitude CA region and smaller for TP and SEA regions. Comparatively, BMA Gaussian mixture PDF of annual total precipitation are generally the same as historical period for the

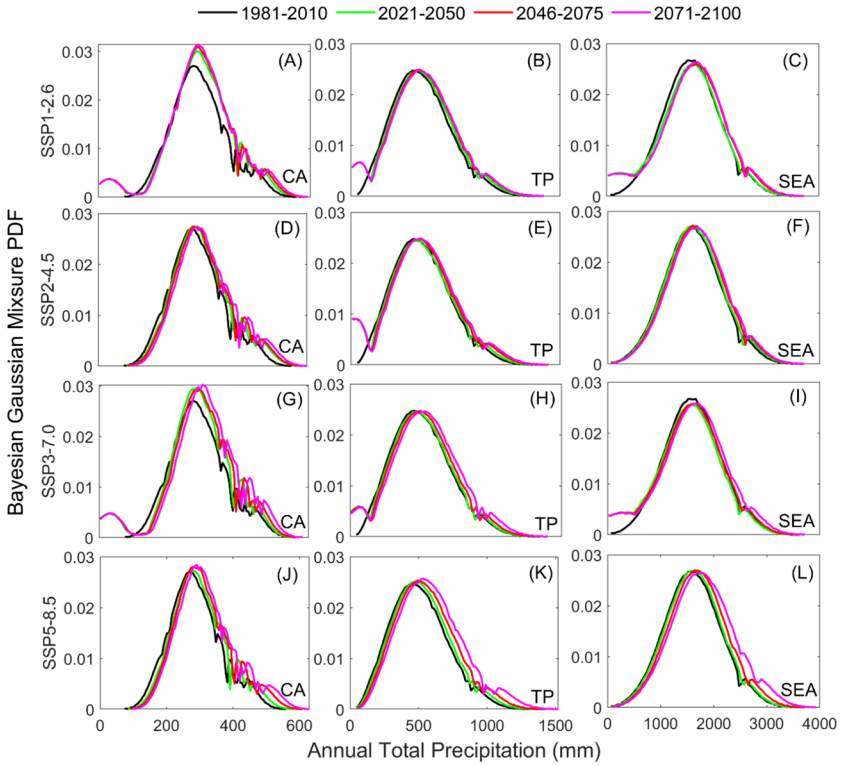

Fig. 14 Bayesian Gaussian mixture probability density function of annual total precipitation under SSP1-2.6 (**A**–**C**), SSP2-4.5 (**D**–**F**), SSP3-7.0 (**G**–**I**) and SSP5-8.5 (**J**–**L**) scenarios for CA, TP and SEA during historical baseline period (1981–2010), near future (2021–2050), middle future (2046–2075) and far future (2071–2100)

future and uncertainty associated with BMA precipitation prediction is higher for low latitude SEA region.

Appendix

Taylor diagram equation

In Taylor diagram, the correlation coefficient, standard deviation and RMSD have the following relationship (Eq. 6):

$$E'^2 = \sigma_M^2 + \sigma_r^2 - 2\sigma_M\sigma_r R \tag{6}$$

where R is the correlation coefficient between the model and reference data. E' is the centered RMSD and σ_M^2 and σ_r^2 are the variances of the model and reference data respectively. In this study, spatial patterns of annual mean temperature and annual total precipitation climatology from CMIP6 and CRU observations are evaluated with Taylor diagram.

Expectation Maximization algorithm

The Expectation Maximization (EM) algorithm is iterative and alternates between two steps, the E (or expectation) step, and the M (or maximization) step by using a latent variable z. In the E step, z is estimated given the current estimates of the model weight w_k and σ_k (Eq. 7). The superscript j refers to the jth iteration of the EM algorithm and is a normal density with mean $M_{k,s}$ and standard deviation . In the M step, the weight w_k and standard deviation σ_k are calculated with the current estimate of $z_{k,s}$ (Eqs. 8 and 9). Where n is the number of observations for distinct values of locations. The E step and M step are iterated to convergence.

$$z_{k,s}^j = \frac{w_k^{j-1} p(y_s|M_{k,s}, \sigma_k^{j-1})}{\sum_{k=1}^K w_k^{j-1} p(y_s|M_{k,s}, \sigma_k^{j-1})} \tag{7}$$

$$w_k^j = \frac{1}{n}\sum_s z_{k,s}^j \tag{8}$$

$$\sigma_k^{2(j)} = \frac{\sum_s z_{k,s}^j (y_s - M_s)^2}{\sum_s z_{k,s}^j} \tag{9}$$

Supplementary information The online version contains supplementary material available at https://doi.org/10.1007/s00382-022-06345-7.

Acknowledgements The authors acknowledge editors and three anonymous reviewers for their constructive comments and suggestions. The authors would also like to acknowledge the World Climate Research Program for managing and providing CMIP6 data and thank Tibet

Plateau Data Center (TPDC) for providing the shapefiles of Tibet Plateau region. This work is supported by Strategic Priority Research Program of the Chinese Academy of Sciences (#XDA20060401), Fundamental Research Funds for the Central Universities (#B220201027), Natural Science Foundation of Jiangsu Province (#SBK2022042221) and National Natural Science Foundation of China (#520007711).

Author contributions ZL: Conceptualization, Methodology, Data acquisition, Software, Writing-original draft. QD: Conceptualization, Funding acquisition, Editing. XF: Data acquisition, Methodology. WL: Data acquisition. JY: Proof reading.

Data availability statement The authors state that the data of this study can be shared based on reasonable request.

Declarations

Conflict of interest The authors declare that no known competing financial interests to influence this study.

References

Balbus JM, Malina C (2009) Identifying vulnerable subpopulations for climate change health effects in the United States. J Occup Environ Med 51(1):33–37

Change C (2007) Climate change impacts, adaptation and vulnerability. Sci Total Environ 326(1–3):95–112

Chen L, Frauenfeld OW (2014) A comprehensive evaluation of precipitation simulations over China based on CMIP5 multimodel ensemble projections. J Geophys Research Atmos 119(10):5767–5786

Cook BI, Mankin JS, Anchukaitis KJ (2018) Climate change and drought: from past to future. Curr Clim Change Rep 4(2):164–179

Diffenbaugh NS, Giorgi F (2012) Climate change hotspots in the CMIP5 global climate model ensemble. Clim Change 114(3):813–822

Du Z, Xiao C, Wang Y, Liu S, Li S (2019) Dust provenance in Pan-third pole modern glacierized regions: what is the regional source? Environ Pollut 250:762–772

Duan Q, Phillips TJ (2010) Bayesian estimation of local signal and noise in multimodel simulations of climate change. J Geophys Res Atmos 115:D18123

Duan Q, Ajami NK, Gao X, Sorooshian S (2007) Multi-model ensemble hydrologic prediction using Bayesian model averaging. Adv Water Resour 30(5):1371–1386

Dufresne J-L et al (2013) Climate change projections using the IPSL-CM5 Earth System Model: from CMIP3 to CMIP5. Clim Dyn 40(9):2123–2165

Eriș MN, Ulașan B (2013) Trade openness and economic growth: Bayesian model averaging estimate of cross-country growth regressions. Econ Model 33:867–883

Eyring V et al (2016) Overview of the Coupled Model Intercomparison Project Phase 6 (CMIP6) experimental design and organization. Geosci Model Dev 9(5):1937–1958

Fan X, Duan Q, Shen C, Wu Y, Xing C (2021a) Evaluation of historical CMIP6 model simulations and future projections of temperature over the Pan-Third Pole region. Environ Sci Pollut Res 29(18):26214–26229

Fan X, Miao C, Duan Q, Shen C, Wu Y (2021b) Future climate change hotspots under different 21st century warming scenarios. Earth Future 9(6):e2021EF002027

Feng Y, He S, Li G (2021) Interaction between urbanization and the eco-environment in the Pan-Third Pole region. Sci Total Environ 789:148011

Harris I, Osborn TJ, Jones P, Lister D (2020) Version 4 of the CRU TS monthly high-resolution gridded multivariate climate dataset. Sci Data 7(1):1–18

Hirabayashi Y et al (2013) Global flood risk under climate change. Nat Clim Change 3(9):816–821

Immerzeel WW, Van Beek LP, Bierkens MF (2010) Climate change will affect the Asian water towers. Science 328(5984):1382–1385

Jiang S et al (2012) Comprehensive evaluation of multi-satellite precipitation products with a dense rain gauge network and optimally merging their simulated hydrological flows using the Bayesian model averaging method. J Hydrol 452:213–225

Knutti R, Rogelj J, Sedláček J, Fischer EM (2016) A scientific critique of the two-degree climate change target. Nat Geosci 9(1):13–18

Li J et al (2021) Evaluation of CMIP6 global climate models for simulating land surface energy and water fluxes during 1979–2014. J Adv Model Earth Syst 13(6):e2021MS002515

Lindvall J, Svensson G (2015) The diurnal temperature range in the CMIP5 models. Clim Dyn 44(1–2):405–421

Liu Z, Merwade V (2018) Accounting for model structure, parameter and input forcing uncertainty in flood inundation modeling using Bayesian model averaging. J Hydrol 565:138–149

Liu Z, Merwade V (2019) Separation and prioritization of uncertainty sources in a raster based flood inundation model using hierarchical Bayesian model averaging. J Hydrol 578:124100

Liu Z, Mehran A, Phillips TJ, AghaKouchak A (2014) Seasonal and regional biases in CMIP5 precipitation simulations. Clim Res 60(1):35–50

Liu Z, Merwade V, Jafarzadegan K (2019) Investigating the role of model structure and surface roughness in generating flood inundation extents using one-and two-dimensional hydraulic models. J Flood Risk Manag 12(1):e12347

Liu Z, Herman JD, Huang G, Kadir T, Dahlke HE (2021) Identifying climate change impacts on surface water supply in the southern Central Valley, California. Sci Total Environ 759:143429

Luan W, Li X (2021) Rapid urbanization and its driving mechanism in the Pan-Third Pole region. Sci Total Environ 750:141270

Lyu K, Zhang X, Church JA (2020) Regional dynamic sea level simulated in the CMIP5 and CMIP6 models: mean biases, future projections, and their linkages. J Clim 33(15):6377–6398

Massoud E, Lee H, Gibson P, Loikith P, Waliser D (2020) Bayesian model averaging of climate model projections constrained by precipitation observations over the contiguous United States. J Hydrometeorol 21(10):2401–2418

Meinshausen M et al (2020) The shared socio-economic pathway (SSP) greenhouse gas concentrations and their extensions to 2500. Geosci Model Dev 13(8):3571–3605

Mustafa SMT, Nossent J, Ghysels G, Huysmans M (2020) Integrated Bayesian Multi-model approach to quantify input, parameter and conceptual model structure uncertainty in groundwater modeling. Environ Model Softw 126:104654

Nasrollahi N et al (2015) How well do CMIP5 climate simulations replicate historical trends and patterns of meteorological droughts? Water Resour Res 51(4):2847–2864

New M, Lister D, Hulme M, Makin I (2002) A high-resolution data set of surface climate over global land areas. Clim Res 21(1):1–25

Raftery AE, Madigan D, Hoeting JA (1997) Bayesian model averaging for linear regression models. J Am Stat Assoc 92(437):179–191

Raftery AE, Gneiting T, Balabdaoui F, Polakowski M (2005) Using Bayesian model averaging to calibrate forecast ensembles. Mon Weather Rev 133(5):1155–1174

Sun Q et al (2020) Possible Increased frequency of ENSO-related dry and wet conditions over some major watersheds in a warming climate. Bull Am Meteorol Soc 101(4):E409–E426

Taylor KE (2001) Summarizing multiple aspects of model performance in a single diagram. J Geophys Research Atmos 106(D7):7183–7192

Tian B, Dong X (2020) The double-ITCZ bias in CMIP3, CMIP5, and CMIP6 models based on annual mean precipitation. Geophys Res Lett 47(8):e2020GL087232

Van Vuuren DP et al (2011) The representative concentration pathways: an overview. Clim Change 109(1):5–31

Vrugt JA, Robinson BA (2007) Treatment of uncertainty using ensemble methods: comparison of sequential data assimilation and Bayesian model averaging. Water Resour Res 43:W01411

Woolway RI et al (2021) Lake heatwaves under climate change. Nature 589(7842):402–407

Yan Z et al (2020) Ensemble projection of runoff in a large-scale basin: modeling with a global BMA approach. Water Resour Res 56(7):e2019WR026134

Yang J, He S, Bao Q (2021) Convective/large-scale rainfall partitions of tropical heavy precipitation in CMIP6 atmospheric models. Adv Atmos Sci 38(6):1020–1027

Yao T et al (2012) Third pole environment (TPE). Environ Dev 3:52–64

Yao T et al (2020) Third Pole climate warming and cryosphere system changes. World Meteorol Organ Bull 69(1):38–44

Yin J, Tsai FT-C (2018) Saltwater scavenging optimization under surrogate uncertainty for a multi-aquifer system. J Hydrol 565:698–710

Yin J, Medellín-Azuara J, Escriva-Bou A, Liu Z (2021) Bayesian machine learning ensemble approach to quantify model uncertainty in predicting groundwater storage change. Sci Total Environ 769:144715

Yue Y, Yan D, Yue Q, Ji G, Wang Z (2021) Future changes in precipitation and temperature over the Yangtze River Basin in China based on CMIP6 GCMs. Atmos Res 264:105828

Zhao D, Wu S (2019) Projected changes in permafrost active layer thickness over the Qinghai-Tibet Plateau under climate change. Water Resour Res 55(9):7860–7875

Zhu Y-Y, Yang S (2020) Evaluation of CMIP6 for historical temperature and precipitation over the Tibetan Plateau and its comparison with CMIP5. Adv Clim Change Res 11(3):239–251